THE JOURNAL OF BIOLOGICAL CHEMISTRY VOL. 281, NO. 50, pp. 38266–38275, December 15, 2006
Printed in the U.S.A.

Solution Structure of Human von Willebrand Factor Studied Using Small Angle Neutron Scattering*[S]

Received for publication, July 26, 2006, and in revised form, October 11, 2006 Published, JBC Papers in Press, October 19, 2006, DOI 10.1074/jbc.M607123200

Indrajeet Singh[‡], Harish Shankaran[‡§], Mark E. Beauharnois[‡], Zhihua Xiao[‡], Paschalis Alexandridis[‡], and Sriram Neelamegham[‡1]

From the [‡]Department of Chemical and Biological Engineering, State University of New York, Buffalo, New York 14260 and the [§]Pacific Northwest National Laboratory, Richland, Washington 99354

von Willebrand factor (VWF) binding to platelets under high fluid shear is an important step regulating atherothrombosis. We applied light and small angle neutron scattering to study the solution structure of human VWF multimers and protomer. Results suggest that these proteins resemble prolate ellipsoids with radius of gyration (R_g) of ~75 and ~30 nm for multimer and protomer, respectively. The ellipsoid dimensions/radii are 175 × 28 nm for multimers and 70 × 9.1 nm for protomers. Substructural repeat domains are evident within multimeric VWF that are indicative of elements of the protomer quarternary structure (16 nm) and individual functional domains (4.5 nm). Amino acids occupy only ~2% of the multimer and protomer volume, compared with 98% for serum albumin and 35% for fibrinogen. VWF treatment with guanidine·HCl, which increases VWF susceptibility to proteolysis by ADAMTS-13, causes local structural changes at length scales <10 nm without altering protein R_g. Treatment of multimer but not protomer VWF with random homobifunctional linker BS^3 prior to reduction of intermonomer disulfide linkages and Western blotting reveals a pattern of dimer and trimer units that indicate the presence of stable intermonomer non-covalent interactions within the multimer. Overall, multimeric VWF appears to be a loosely packed ellipsoidal protein with non-covalent interactions between different monomer units stabilizing its solution structure. Local, and not large scale, changes in multimer conformation are sufficient for ADAMTS-13-mediated proteolysis.

von Willebrand factor (VWF)[2] is a large, multidomain glycoprotein that is present in human blood and in secretory granules of endothelial cells and platelets (1–3). This protein occurs both as a protomer and in multimeric form. The ~500-kDa protomer consists of two identical monomer subunits linked at the C terminus by disulfide bonds. Linear multimers formed by cysteine-cysteine linkages near the N terminus result in a molecular mass of >10,000 kDa.

VWF serves many functions. The binding of surface-immobilized VWF to platelet receptor GpIbα results in intermolecular bonds with high tensile strength (4, 5). This molecular interaction allows platelet capture at sites of vascular injury under high fluid shear conditions. The binding of plasma VWF to platelet receptor GpIbα under high hydrodynamic shear also leads to platelet activation and subsequent platelet arrest (6). Various mutations in VWF result in the bleeding defects that characterize von Willebrand disease (1). In blood, VWF binding to pro-coagulation factor VIII increases factor VIII lifetime in circulation. Finally, the size of VWF and its response to fluid flow are key determinants in regulating protein function under physiological and pathological conditions. In support of this, the life threatening systemic illness thrombotic thrombocytopenic purpura (TTP) is attributed to the presence of very large VWF multimers, which are caused by the malfunction or absence of a metalloprotease termed ADAMTS-13 ("a disintegrin and metalloprotease with thrombospondin" family member) (7) VWF cleavage by ADAMTS-13 is enhanced both upon protein denaturation with guanidine·HCl (Gd·HCl) (8) and upon application of physiological fluid shear (9).

Structural studies on VWF have been performed using two-dimensional electron microscopy (10–12). These studies show that multimeric VWF consists of a repeating protomer unit that has a maximum extended length of 120 nm (12) (Fig. 1). This protomer has 2-fold symmetry, with each half consisting of a long flexible 34 × 2-nm rod linked to a large globular 22 × 6.5-nm domain at one end and to a second rod at the other end. Using rotary-shadowed electron microscopy of VWF deposited on mica surfaces, it has been shown that whereas 87% of multimeric VWF adopt a "ball of yarn" or "tangled" conformation with a mean diameter of 100–150 nm, the remaining exist in an "extended form" with a mean length of 350 nm (10). Atomic force microscopy (AFM) measurements of VWF immobilized on different substrates further suggest that the VWF structure determined using microscopy depends on the surface on which it is deposited. On hydrophobic octadecyltrichlorosilane-modified glass, VWF exhibits a compact structure, whereas the molecule is more extended on hydrophilic mica (13).

The detailed solution structure of VWF is yet to be determined. Whereas light scattering provides good estimates of hydrodynamic radius (R_h) and radius of gyration (R_g), this method does not provide detailed information on molecular

* This work was supported by National Institutes of Health Grants HL76211 and HL77258. The costs of publication of this article were defrayed in part by the payment of page charges. This article must therefore be hereby marked "*advertisement*" in accordance with 18 U.S.C. Section 1734 solely to indicate this fact.

[S] The on-line version of this article (available at http://www.jbc.org) contains supplemental Figs. S1–S4 and supplemental methods.

[1] To whom correspondence should be addressed: 906 Furnas Hall, State University of New York, Buffalo, NY 14260. Tel.: 716-645-2911 (ext. 2220); Fax: 716-645-3822; E-mail: neel@eng.buffalo.edu.

[2] The abbreviations used are: VWF, von Willebrand factor; SANS, small angle neutron scattering; Gd·HCl, guanidine·HCl; Gd·DCl, deuterated Gd·HCl; R_g, radius of gyration; D_h, hydrodynamic diameter; q, scattering vector; BS^3, bis[sulfosuccinimidyl]suberate; Ab, antibody; FITC, fluorescein isothiocyanate; DTT, dithiothreitol; BSA, bovine serum albumin.

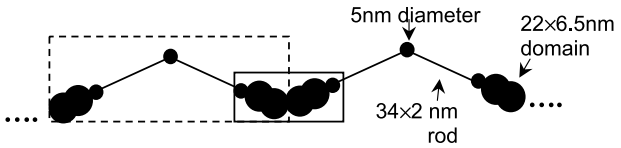

FIGURE 1. **Schematic of VWF.** Two adjacent protomers of a larger VWF multimer are shown in extended form along with dimensions measured using electron microscopy by Fowler *et al.* (12). *Dashed box* indicates a single protomer unit. *Smaller box* indicates globular domain located at the intersection of adjacent protomer units.

shape (12, 14, 15). X-ray crystallography data have allowed structural characterization of individual protein domains either alone (16, 17) or when in complex with antibodies (17) botrocetin (18) or GpIbα receptor (19). Such data, however, only provide a static picture of individual domains and not the dynamic features of the full soluble protein. To address this gap in knowledge, we performed light and small angle neutron scattering (SANS) studies with human multimeric VWF isolated from plasma cryoprecipitate and recombinant protomer VWF expressed in mammalian systems. These methods probe protein structure over a wide length scale from 2 to 250 nm. Thus, they allow the simultaneous study of specific treatments on both the domain structure and overall protein shape. We observed that both multimer and protomer VWF exist as prolate ellipsoids with R_g of ~75–100 nm and 30 nm, respectively. Structural studies with the denaturant Gd·HCl suggest that large scale changes in protein structure are not necessary for proteolysis by ADAMTS-13. Thus, fluid shear in previous studies (9) may cause subtle rearrangement of VWF domains rather than unraveling the entire protein. Cross-linking studies with amino homobifunctional cross-linker BS^3 (bis[sulfosuccinimidyl]suberate) also reveal, for the first time, that VWF solution structure is stabilized by frequent interdomain interactions between residues located on different monomer units. Such interdomain interactions may be important regulators of VWF function in normal physiology and pathology.

EXPERIMENTAL PROCEDURES

Materials—Polyclonal rabbit antihuman VWF was from Dako (Carpinteria, CA). Non-inhibitory anti-VWF mAb AVW-1 and A1 domain function blocking mAb AVW-3 were from GTI Diagnostics (Waukesha, WI). Polyclonal rat antifactor VIII antibody and recombinant factor VIII were kindly provided by Dr. Balasubramanian (SUNY-Buffalo). $F(ab')_2$ Alexa 488-conjugated secondary antibodies were from Invitrogen. All chemicals were from Sigma unless otherwise specified.

Denaturant Gd·HCl was deuterated by dissolving it in 99.9% D_2O (Cambridge Isotope, Andover, MA) at 4 M and subjecting the solution to three cycles of evaporation using a vacuum oven, with resuspension in D_2O at the end of each cycle (20). The final product, which is abbreviated Gd·DCl, was completely deuterated as determined by proton NMR spectroscopy (Varian Inova-500, Fort Collins, CO) and solid phase fourier transform infrared spectroscopy (Mattson Galaxy series FT-IR 5000, Madison, WI).

Multimeric human VWF was purified from blood plasma cryoprecipitate obtained from Community Blood Bank (Erie, PA) (14). Silver staining of SDS-PAGE gels confirmed that a unique protein was isolated.

VWF Protomer (ΔPro-VWF) Expression—Full-length VWF contains 2813 amino acids including a 741-amino acid propeptide. Deletion of this propeptide results in dimeric ΔPro-VWF formation with protomer units linked by disulfide bonds at the C, but not N terminus (21). To produce ΔPro-VWF for small angle scattering studies, cDNA was purchased from ATCC (Manassas, VA) in the PMT-2-ADA vector. This construct was digested with EcoRI, and full-length VWF was cloned into pcDNA3.1(+)/Myc-His (Invitrogen, Carlsbad, CA) (VWF-pcDNA). VWF-pcDNA was then digested using BamHI, and the excised fragment of VWF was ligated into pBluescript sk(+) (Stratagene). The propeptide portion of VWF (residues Ala^{23}-Arg^{763}) was deleted in this vector by performing a PCR with 5′-phosphate sense 5′-AGCCTATCCTGTCGGCCtCCaATGGTCAAGCTG-3′ and antisense 5′-ACAAAGGGTCCCTGGCAAAATGAG-3′ primers. During this PCR step, silent mutations at C2307T and C2310A were introduced to facilitate primer design. The PCR product thus formed was purified and blunt end-ligated (del-BamHI-VWF-Blue). del-BamHI-VWF-Blue was digested with BamHI, and the VWF fragment was ligated back into the BamHI-digested VWF in pcDNA (ΔPro-VWF-pcDNA). Restriction enzyme digests were performed to verify correct orientation of insert, and the final product was sequenced.

CHO-S cells (Invitrogen) were transfected with ΔPro-VWF-pcDNA using FuGENE 6 (Roche Applied Sciences, Indianapolis, IN) according to the manufacturer's instructions. Stable clones were obtained by selecting with 2 mg/ml G418 (Invitrogen). After selection, the antibiotic concentration was reduced to 0.5 mg/ml. Unique colonies were obtained by limiting dilution and were then scaled up for protein purification. The cultures were converted to protein-free CD-CHO media (Invitrogen), and the cell culture supernatant was harvested for ΔPro-VWF purification.

A two-step procedure was used to purify ΔPro-VWF from CD-CHO culture medium. In the first step, anion exchange chromatography was applied using Fractogel® EMD TMAE (M) (EMD Chemicals, Gibbstown, NJ) and FPLC system from Amersham Biosciences/GE Healthcare Biosciences (Piscataway, NJ) (22). This column was first equilibrated with 20 mM Tris buffer, pH 7.4. Cell culture supernatant containing ΔPro-VWF was diluted 1:1 in 20 mM Tris buffer (final pH 7.2), and this was run through the column twice. VWF binding to column was verified by assaying negligible VWF concentration in culture supernatant following passage through ion-exchange column, using the flow cytometry-based VWF concentration assay described below. Following binding, VWF was eluted using 20 mM Tris buffer by increasing NaCl concentration in a stepwise manner from 150 and 260 mM up to 400 mM. VWF was observed to elute when 260 mM NaCl was applied. Fractions containing ΔPro-VWF were thus pooled. In the second step, Microsep™ 100-kDa cutoff centrifugal devices (Pall Life Sciences, Ann Arbor, MI) were used to remove low molecular weight impurity. First a 15-fold concentration of the pooled fractions was performed. Following this, two more sequential cycles of centrifugal concentration were performed with ΔPro-VWF, with protein volume increased by 10-fold using 20 mM Tris buffer before each centrifugation step, and 10-fold concen-

tration was accomplished. Fresh Microsep units were used for each centrifugal concentration step. Following the third and final centrifugal step, theoretically, >99% of the low molecular impurities should have been removed.

Protein Concentration Determination—VWF concentration was measured using three methods. In the case of purified protein where concentration was high (>1–2 μg/ml), the Coomassie/Bradford protein assay kit (Pierce) was employed.

In complex protein mixtures and at lower concentrations down to 50 ng/ml, VWF concentration was assayed using a flow cytometry assay. For this, mAb AVW-1 was covalently immobilized on 5.7-μm polybead-carboxylated microbeads (Polysciences, Warrington, PA) using carbodiimide chemistry (23). These beads are called anti-VWF beads. Polyclonal anti-VWF mAb (Dako) was conjugated with FITC. Multimeric VWF protein standards were also developed for this assay based on measurement of protein concentration using the Coomassie protein assay kit. During each run, VWF (unknown samples or standards at varying doses) was incubated with 10^6 anti-VWF beads/ml for 20 min at room temperature, washed, and then l:20 (v/v) FITC-conjugated polyclonal anti-VWF was added to these beads. Following 20 min, the sample was again washed. FITC fluorescence associated with the beads was then measured by FACSCalibur flow cytometry (BD Biosciences, San Jose, CA) to quantify VWF concentration. As shown in supplemental Fig. S1, this assay detected protein concentration down to ~50 ng/ml, and sample readouts were linear over at least two logs (0.1–10 μg/ml).

Quantitative amino acid analysis was further performed at the Protein Chemistry Laboratory (Texas A&M University), and results from this absolute measurement were used to calibrate both the Bradford and flow cytometry assays described above. Thus, the VWF concentrations presented in this article are based on amino acid analysis. Here, we observed that the Bradford assay overpredicts VWF concentration by ~6%. The concentration of individual amino acids assayed using amino acid analysis was also within 10% of that predicted based on protein primary sequence. This is reasonable for a purified protein.

Electrophoresis—Western blotting of VWF was performed using 0.6% agarose gel (14). Silver staining of gradient (4–20%) SDS-PAGE gels was performed using Silver SNAP stain Kit II (Pierce). Densitometry analysis was performed using the Kodak 1-D software (New Haven, CT).

In studies with BS^3, the homobifunctional cross-linker was dissolved in Hepes buffer (30 mM Hepes, 110 mM NaCl, 10 mM KCl, 1 mM $MgCl_2$, 10 mM glucose, pH 7.3) immediately prior to use. This was added to either 9.4 μg/ml or 47 μg/ml VWF at either 1 or 5 mM concentrations for fixed times. The reaction was then quenched using 40 mM Tris (pH 7.5) for 15 min, and disulfide bonds were reduced by adding 25 mM DTT (dithiothreitol) for 30 min. This was followed by Western blot analysis. Protein mass was estimated using fibrinogen, IgM, and ΔPro-VWF, in addition to ladders from Bio-Rad.

Factor VIII Analysis—The function of the D′ domain in multimeric and promoter VWF was confirmed by measuring factor VIII binding to VWF. For studies with multimeric VWF, the amount of factor VIII bound to VWF during its purification from plasma cryoprecipitate was determined using a one-stage activated partial thromboplastin time (aPTT) assay using micronized silica as an activator (Organon Teknika Corporation, Durham, NC) and factor VIII-deficient plasma (Biopool International, Ventura, CA) as substrate. The assay was performed using COAG-A-MATE coagulation analyzer (Organon Teknika). Purified VWF samples or factor VIII standards were added to factor VIII-deficient plasma, and the clotting time was monitored. The factor VIII concentration in VWF samples was obtained by comparing the clotting time to those of recombinant factor VIII standards.

To confirm that factor VIII binds recombinant ΔPro-VWF, a "sandwich-cytometry" assay was developed. For this, polyclonal rabbit antihuman VWF mAb was covalently immobilized on 5.7-μm carboxylate polystyrene beads using carbodiimide chemistry (23). Plasma VWF from cryoprecipitate (0.57 μg/ml) or ΔPro-VWF (1.53 μg/ml) were incubated with these beads (10^6/ml) along with either 10 μg/ml mouse anti-VWF mAb (clone AVW-3) and 1:200 polyclonal anti-mouse Alexa488-conjugated Ab to quantify VWF bound on beads; or with 7.5 μg/ml recombinant factor VIII along with 1:100 polyclonal anti-factor VIII rat antibody and 1:200 Alexa488-conjugated detection secondary Ab to quantify factor VIII associated with beads. Following 30 min of incubation in the dark, the sample volume was increased 25-fold, and binding of VWF and factor VIII to beads was independently determined using flow cytometry measurement based on Alexa488 fluorescence associated with beads. Control beads were prepared identically as above, except they lacked immobilized VWF. Fluorescence of controls was subtracted from sample fluorescence for data presented here.

VWF-GpIbα Binding—The function of the A1 domain of multimeric and protomer VWF was measured by either assaying the ability of multimeric VWF to function in a shear-induced platelet activation assay (14) or by measuring the binding of recombinant protein to platelet GpIbα under fluid flow conditions. The methods for the platelet activation assay are described elsewhere (14). Here, multimeric VWF isolated from plasma cryoprecipitate was observed to behave similarly to native protein in human blood in terms of its ability to bind platelet GpIbα and activate platelets.

For the binding assay, 9.4 μg/ml VWF (ΔPro-VWF or purified multimeric VWF) was incubated with 10^6/ml anti-VWF beads (described above) for 20 min. This resulted in VWF immobilization on polystyrene beads. Platelets isolated from human blood were labeled green using a FITC-conjugated anti-CD61/GpIIIa Ab (Dako) as previously described (23). Following this, 5×10^6 beads/ml were mixed with 15×10^6 platelets/ml in a cone-plate viscometer at a shear rate of 1785/s. Samples withdrawn at 60 s were analyzed using flow cytometry to measure percent bead-platelet adhesion, which is defined as percent of beads having at least one platelet bound to it. The specificity of the interaction was confirmed both using control beads without immobilized VWF and using function blocking anti-VWF mAb, AVW-3.

Small Angle Neutron Scattering—Multimeric and protomer VWF were dialyzed three times against Hepes buffer (composition given above) that lacked glucose and that was made in

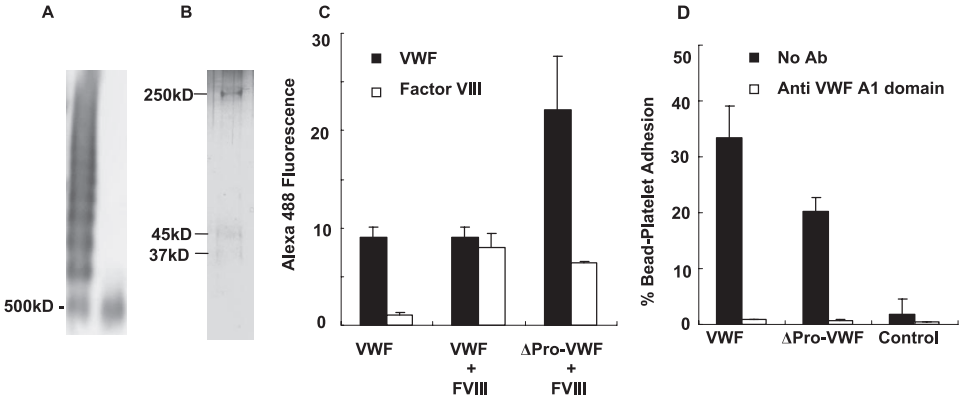

FIGURE 2. **Purification and characterization of ΔPro-VWF.** *A*, Western blot analysis of multimeric VWF (*lane 1*) and ΔPro-VWF (*lane 2*) performed by electrophoresis on 0.6% agarose gel, followed by transfer onto a 0.4-μm nitrocellulose membrane and detection using polyclonal anti-VWF antibody. *B*, silver stain of purified ΔPro-VWF on a gradient (4–20%) SDS-PAGE gel. ΔPro-VWF was reduced with 25 mM DTT for 30 min prior to electrophoresis. Densitometry analysis of the gel suggests that ~93% of reduced protein corresponds to VWF monomer at 250 kDa. Smaller mass proteins (<7%) appear to be non-covalently associated with VWF, because these could not be removed even after three cycles of centrifugal filtration using a 100-kDa cut-off membrane. *C*, sandwich-cytometry assay was applied to measure factor VIII binding to VWF. 0.57 μg/ml multimeric plasma VWF or 1.53 μg/ml ΔPro-VWF was incubated with 10^6/ml polystyrene beads bearing polyclonal anti-human VWF Ab. 7.5 μg/ml exogenous recombinant factor VIII was added in some runs. VWF bound to beads was detected using anti-VWF mAb AVW-3 (*black bar*), and factor VIII binding was measured using polyclonal anti-Factor VIII Ab (*white bar*). The amount of VWF and factor VIII bound to beads is presented in arbitrary fluorescence units measured using flow cytometry, after subtraction of fluorescence of control beads that were treated identically to sample, except that they were not incubated with VWF. VWF from plasma cryoprecipitate had low levels of factor VIII bound to it, but this protein bound 3-fold greater amounts of factor VIII than ΔPro-VWF when exogenous factor VIII was added. *D*, 9.4 μg/ml multimeric plasma VWF or ΔPro-VWF were immobilized on anti-VWF beads. These beads were shear mixed with platelets, which were labeled green using anti-CD-61 FITC mAb, in a cone-plate viscometer at 1785/s. % of single beads with at least one bound platelet was determined using flow cytometry at the 60s time point. Blocking mAb against the A1 domain (clone AVW-3) was used to confirm the specificity of the molecular interaction. Control beads did not have any immobilized VWF. *Error bars* are S.E. for $n = 2–6$.

99.9% D_2O. The goal of this dialysis was to remove residual hydrogenated material that can contribute to the incoherent scattering of neutrons. Detailed methods including instrument settings and data analysis protocols are provided under supplemental materials. A brief overview follows.

SANS measurements were performed on the 30-m NG3 SANS spectrometer at the NIST Center for Neutron Research (Gaithersburg, MD) (24). During experimentation, 0.094–0.28 mg/ml multimeric or 0.15 mg/ml protomer VWF was placed in the path of a 6-Å neutron beam at room temperature. In some runs, VWF was incubated with 1.25 M Gd·DCl for 4–5 h before SANS measurement. SANS experiments produce data that quantify scattering intensity, $I(q)$, as a function of the scattering vector, q. In general, q is a measure of instrument magnification (25), and it is defined as $4\pi/\lambda\sin(\theta/2)$, with θ representing the scattering angle and λ the neutron wavelength. Because scattering angle (θ) is related to the macromolecule length scale under study, the $I(q)$ *versus* q plot contains information on protein solution structure. The q range applied in our experiments allows study of proteins in the size range from 2–250 nm.

SANS data were analyzed using three complementary approaches. First, VWF R_g was estimated by plotting $1/I(q)$ *versus* $q^{2.206}$, and fitting data using the Calmettes approximation (26). Only a few points at the lowest q range were used for this analysis because this analysis method is only valid when $qR_g < 4$. The intercept of this plot yields $1/I(0)$, and R_g is obtained using $R_g = (3 \times \text{slope}/(0.359 \times \text{intercept}))^{1/2.206}$. Second, the overall protein shape was determined by fitting the $I(q)$ *versus* q data in the low and moderate q range, with the model of an ellipsoid using software available from NIST. Output parameters from this fit were the major and minor axis radii, r_a and r_b. The radius of gyration R_g was calculated using $R_g = r_b[(\nu^2 + 2)/5]^{0.5}$, and this was within 20% of the value obtained from Calmettes analysis. Finally, higher resolution fitting of data over the entire q range was performed using the unified equation (27). According to this, scatter arising from a complex morphology over a wide q range is the result of individual contributions from substructural elements that span a smaller q range. In this context, each structural level resembles a plateau at low q in the $I(q)$ *versus* q plot followed by a power law decay at higher q (27). The scattering intensity at the low q plateau is defined by the parameter G_i (Guinier prefactor), the point where the decay begins is defined by R_{gi} (R_g of the i^{th} structural level) and P_i (power law exponent) defines the decay-slope at high q. G_i is thus a measure of neutron intensity at the start of the i^{th} structural feature, and it equals $I(0)$ in the case of the first structural level. Depending on protein concentration and extent of VWF multimer formation, G for lower structural levels can differ between different VWF preparations. P_i contains information about the features of the substructure: $4 > P_i > 3$ for surface fractals, $P_i < 3$ for mass fractals, and $P_i > 4$ for diffuse interfaces. Radii of consecutive structural levels (R_{gi} and $R_{g(i+1)}$) define the bounds of each structural level. Using a piecewise fitting algorithm described under supplemental materials, G_i, R_{gi}, and P_i were determined for substructures that form multimeric and protomer VWF.

Dynamic Light Scattering—Dynamic light scattering experiments were performed using a Brookhaven Goniometer (BI-200SM Ver.2.0, Brookhaven Instruments, Holtsville, NY) with a 514-nm laser and autocorrelator (model:BI-9000AT) (14). These experiments yielded VWF hydrodynamic diameter distribution function on a volume basis.

Statistics—All data are presented as mean ± S.E., except for SANS data where error bars represent S.D.

RESULTS

Light and neutron scattering studies were performed with protomer and multimeric VWF. Efforts were undertaken to characterize the protein function so that structural results could be attributed to functional macromolecules.

Functional Characterization of Protomer VWF (ΔPro-VWF)—For studies with ΔPro-VWF, this protein was expressed in stably transfected mammalian CHO cells. After scale up, the flow cytometry-based protein assay demonstrated that the cell cul-

ture supernatant of transfected CHO cells yielded ΔPro-VWF at ~1.88 μg/ml. This was purified and concentrated to 150 μg/ml. Fig. 2*A* compares the Western blots for multimeric and ΔPro-VWF. As seen, ΔPro-VWF has a molecular mass of ~500 kDa, which corresponds to the lowest mass band of the multimeric protein. Mutimeric VWF preparations had a size up to 20–30 mers as determined using densitometry. Silver staining and densitometry analysis of reduced ΔPro-VWF (~250 kDa in Fig. 2*B*) demonstrated this protein was ~93% pure. Lower density bands of 45 and 37 kDa were also present. The lower mass bands remain even after repeated centrifugal filtration, suggesting that these were non-covalently associated with VWF when the protein was secreted from CHO cells. Addition of DTT and SDS prior to electrophoresis likely resulted in their dissociation from VWF. There is a minimal contribution of lower MW proteins to ΔPro-VWF scattering data as discussed later.

ΔPro-VWF was functional in terms of its ability to bind factor VIII (Fig. 2*C*). In this sandwich-cytometry assay, which independently measured the binding of VWF to anti-VWF beads and of factor VIII to VWF immobilized on these beads, we determined that multimeric VWF from plasma cryoprecipitate had low levels of factor VIII bound to it. This is consistent with dissociation constant (K_D = 0.4 nM) and off-rate (k_{off} = 2.3×10^{-4}/s) measurements for factor VIII-VWF interaction (28). Based on these binding affinities, it is expected that whereas factor VIII is bound to VWF during protein isolation from blood, it may have dissociated over a period of days prior to the experiments described here. Indeed, factor VIII binding to multimeric VWF could be readily restored upon addition of recombinant exogenous factor VIII. The multimeric protein bound factor VIII more efficiently than dimeric ΔPro-VWF, suggesting that the multimeric nature of VWF may enhance binding interactions.

The function of the A1-domain of ΔPro-VWF was confirmed using a platelet-VWF bead adhesion assay under shear (Fig. 2*D*). Here, platelets were observed to readily engage VWF-bearing beads when fluid shear rate was applied at 1785/s. Specificity was confirmed using blocking antibody against VWF A1-domain.

ΔPro-VWF Has an R_g of 30 nm and 4.5-nm Subdomains—Light scattering and SANS studies were performed with purified dimeric ΔPro-VWF to characterize its solution structure. Dynamic light scattering showed that protein hydrodynamic diameter D_h varied from 15–50 nm (Fig. 3*A*). Similar values of D_h were obtained when protein concentration was varied from 37 to 150 μg/ml, suggesting that these measurements are reliable. The relatively narrow distribution of D_h values suggests that ΔPro-VWF may not aggregate spontaneously in solution.

SANS analysis of ΔPro-VWF was performed. Calmettes analysis (26) of SANS data at $q < 0.09$/nm (Fig. 3*B*) yields an $I(0)$ value of 0.19/cm and R_g of 32.6 nm. Using these estimates as a starting point, SANS data over the entire q range were fit to the model of a monodispersed ellipsoid (Fig. 3*C*). A prolate ellipsoid (shape of an elongated rugby ball) with R_g, r_a, and r_b values of 31.8, 70.0, and 9.1 nm, respectively, fit the data well at $q <$ 0.2/nm. These parameter values are in reasonable agreement with previous electron microscopy measurements of protomer units (12). Because SANS data contain information over different length scales, the unified equation was next used to fit data over the entire q range (Fig. 3*D*). Two different structural levels were observed. The first level, which represents the overall structure of ΔPro-VWF, has G_1, $R_{g,1}$, and P_1 values of 0.3/cm, 30 nm, and 2.4, respectively. The smaller structural level has G_2, $R_{g,2}$, and P_2 values of 0.025/cm, 4.5 nm, and 3.0. This substructure may represent individual protein domains because the A1 and A3 domains of VWF are known to exist in the size range of 4 nm (16, 29). In addition, this substructure may also include information on the nature of interaction between protein domains. Because $P_i \leq 3$ for both structural levels above, the structure of VWF has the features of a mass fractal (27). Upon considering ellipsoid dimensions of ΔPro-VWF and volume occupied by amino acids based on protein molecular composition (30), it is estimated that only ~2% of the ellipsoid is occupied by protein mass, whereas the remaining is water (supplemental materials). ΔPro-VWF is thus loosely packed compared with other proteins like BSA and fibrinogen (see "Discussion").

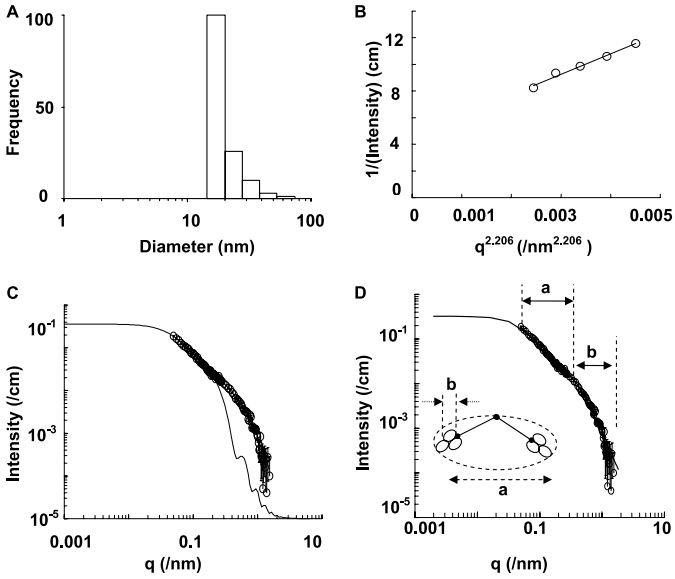

FIGURE 3. **Protomer VWF light and neutron scattering.** *A*, dynamic light scattering studies of ΔPro-VWF revealed hydrodynamic diameter D_h in the range 15–50 nm. *B*, Calmettes plot generated with SANS data points at $q <$ 0.09/nm provide $I(0)$ values of 0.19/cm and R_g of 32.6 nm. *C*, $I(q)$ *versus* q (q range = 0.05–1.8/nm) from SANS study of protomer VWF. As seen in the model fit, at large length scales (low/moderate q), VWF resembles a prolate ellipsoid with R_g = 31.8 nm, r_a = 70 nm, and r_b = 9.1 nm. *D*, unified equation fit data over the entire q range when two structural levels were accounted for. *Level a* represents information about the entire ΔPro-VWF whereas *b* provides information on smaller structural features at R_g ~ 4.5 nm (as shown in the schematic). *Discrete points* represent experimental data in all panels whereas *smooth lines* are model fits.

Functional Characterization of Multimeric VWF—Studies were next performed to relate scattering data of individual protomers to their arrangement in multimers. As part of this investigation, experiments were performed to confirm that the multimeric protein in our studies exhibited activity similar to plasma VWF. In the aPTT assay (Table 1), we determined the amount of factor VIII associated with VWF during protein isolation from plasma cryoprecipitate. These studies showed that a single factor VIII molecule was bound to ~30–200 VWF protomers in both purified VWF and blood plasma. These results are consistent with the published data (31). The isolated VWF

was also active in terms of its ability to bind platelet receptor GpIbα via its A1 domain and to activate platelets in a shear-induced platelet activation assay (see earlier publication, Ref. 14). In a final assay performed to confirm the function of purified multimeric protein, we determined that multimeric VWF did not undergo proteolysis by ADAMTS-13 unless this protein was denatured using Gd·HCl (supplemental Fig. S2). These studies confirm both the presence of functional VWF and the absence of denatured protein in our preparation.

TABLE 1
Factor VIII content in purified multimeric VWF obtained from three donors

Sample	Number of VWF protomers per factor VIII molecule[a]
Plasma	36.5 ± 0.051
B^+ VWF	221.9 ± 14.4
O^+ VWF	51.4 ± 0.35
A^+ VWF	46.1 ± 1.1

[a] Data are mean ± S.E.

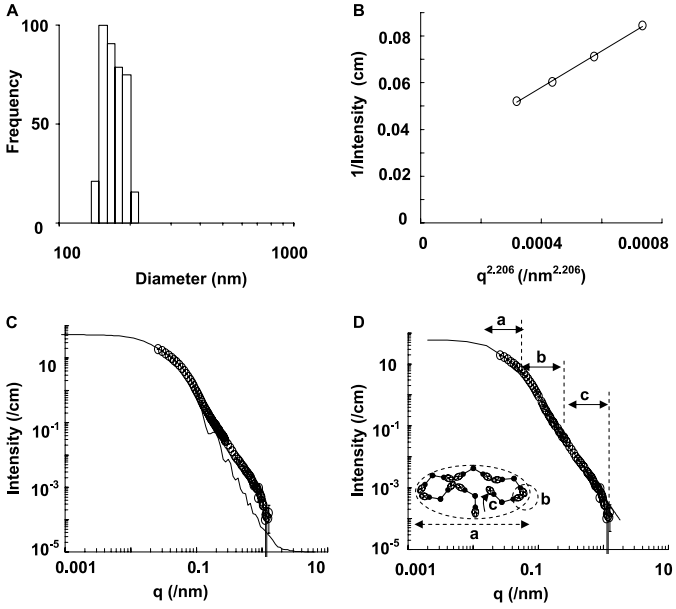

FIGURE 4. **Multimer VWF light and neutron scattering.** *A*, dynamic light scattering shows that the hydrodynamic diameter of multimeric protein lies between 130 and 200 nm. *B*, Calmettes analysis of SANS data at $q < 0.04$/nm yields a multimeric VWF R_g of 97.3 nm. *C*, *I*(*q*) *versus q* SANS data for multimeric protein is shown in the *q* range from 0.03/nm to 1.8/nm. Analysis using ellipsoid model shows that VWF is best fit by a prolate ellipsoid with major and minor axes of 175 nm and 28 nm, and R_g of 80.2 nm. *D*, unified equation fit reveal three distinct structural levels (*a*, *b*, and *c*) within multimeric protein. *Level a* is the multimeric molecule with R_g ~75 nm, *level b* is an intermediate structure, smaller than the protomeric unit with R_g ~16 nm. This probably represents the globular domain at the N terminus of VWF. *Level c* represents smaller structural features at R_g ~ 4.5 nm. *Discrete points* represent experimental data in all panels whereas *smooth lines* are model fits.

Three Distinct Substructures Contribute to VWF Solution Conformation—Light and neutron scattering studies were undertaken with multimeric protein. Unlike the protomer, dynamic light scattering experiments showed that the hydrodynamic diameter of multimeric VWF (D_h) varied over a range from 130 to 200 nm (Fig. 4*A*). This is indicative of VWF polydispersity. Calmettes analysis of SANS data at $q < 0.04$/nm resulted in $I(0)$ values of 37.3 and R_g of 97.3 nm (Fig. 4*B*). These estimates of R_g are in agreement with previous results (14). Using the above $I(0)$ value, we observed that SANS data at $q <$ 0.1/nm could be fit to a prolate ellipsoid with major and minor axis radius values of 175 and 28 nm (Fig. 4*C*).

Fig. 4*D* presents the unified equation fit. Three different structure levels were observed with multimers at R_g of ~75 nm, intermediate structures at R_g ~ 16 nm, and domain level structural features at R_g ~ 4.5 nm. The 16-nm intermediate level likely represents the protomeric globule structure formed at the N terminus of two adjacent VWF monomers, as illustrated in the figure inset (12). Table 2 presents unified equation parameter values for 11 independent VWF samples analyzed using SANS. Some of these samples were from a single individual whereas others were pooled samples. Three structural levels were consistently observed in each of these samples with similar $R_{g,i}$ and P_i values. This confirms that data presented in Fig. 4*D* are donor- and blood group-independent. The ratio of G_2/G_3 were constant at ten among the samples, because similar domain structures contribute to protomer structure in each protein. Further, some variation in the ratio of G_1/G_2 was noted (162.5 ± 19.4), and this reflects the different multimer distribution in each sample. Finally, the absolute value of G_1 varied because this was a function of protein concentration in addition to VWF size.

Guanidine·HCl Causes Local Changes in VWF Domain Structure without Altering Overall Shape or Size—We tested the ability of SANS to identify structural changes in VWF, because such analysis can aid future structure-function investigations. The deuterated denaturant Gd·DCl was used in these runs (Fig. 5), because treatment of VWF with this denaturant enhances VWF susceptibility to proteolytic cleavage by ADAMTS-13 (8). As seen, the R_g of the multimer did not change upon denaturant treatment, whereas the slope of the scattering curve at the highest q was reduced. This change in slope at length scales <10 nm supports the proposition that

TABLE 2
Unified equation fit to SANS data for 11 different VWF preparations

VWF sample number	G_1	$R_{g,1}$	P_1	G_2	$R_{g,2}$	P_2	G_3	$R_{g,3}$	P_3
	/cm	nm		/cm	nm		/cm	nm	
1	16	75	2	0.13	16	2.4	0.013	4.5	3
2	8	75	2	0.04	15	2.4	0.004	4.5	3
3	60	75	2	0.25	15	2.4	0.025	5.0	3
4	13	75	2	0.05	15	2.4	0.005	4.5	3
5	11	75	2	0.06	16	2.6	0.006	4.5	3
6	50	75	2	0.4	16	2.4	0.04	4.5	3
7	15	75	2	0.25	17	2.4	0.025	4.5	3
8	20	75	2	0.22	17	2.4	0.022	4.5	3
9	125	75	2	0.55	16	2.4	0.055	4.5	3
10	80	60	2	0.55	17	2.4	0.055	4.5	3
11	40	75	2	0.3	17	2.4	0.03	4.5	3

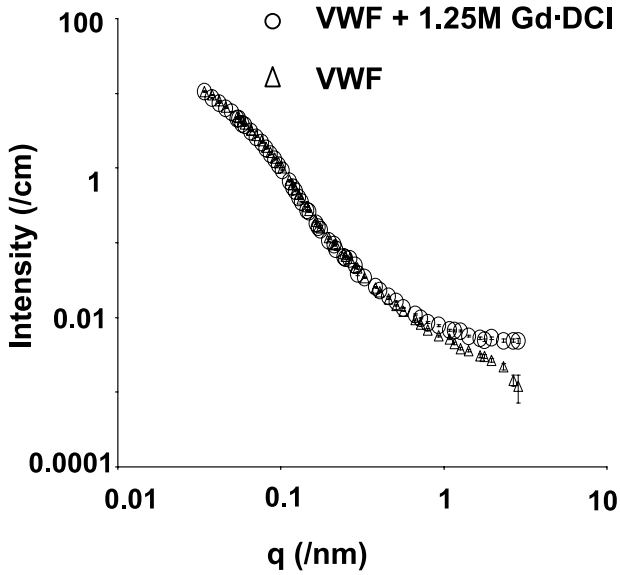

FIGURE 5. **Effect of denaturant Gd·DCl on VWF multimer.** SANS data for multimeric VWF before and after treatment with 1.25 M Gd·DCl. Gd·DCl does not affect the R_g of the protein, though it alters structural features at length scales <10 nm. Data are representative of three independent experiments with VWF from different donors.

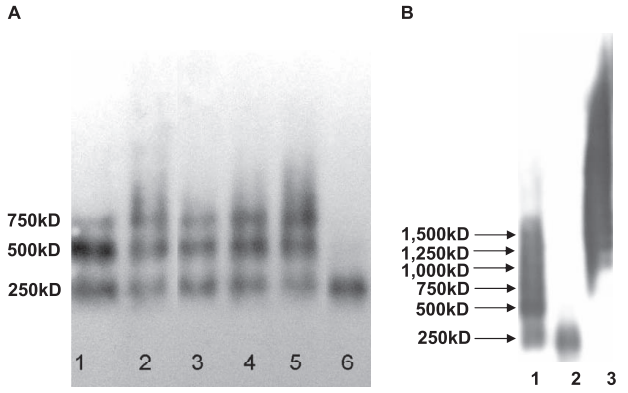

FIGURE 6. **Domain-domain interactions within VWF multimers.** *A*, pooled VWF sample consisting of both low and high molecular mass multimers was treated with homobifunctional cross-linker BS^3, which links proximal amine residues randomly, prior to reduction using DTT and Western blot analysis. In *lane 1*, 9.4 μg/ml VWF was sequentially treated with 1 mM BS^3 for 30 min, 40 mM Tris (excess amine) for 15 min, and 25 mM DTT for 30 min prior to Western blot analysis. *Lane 2* is the same as *lane 1* only BS^3 concentration used was 5-fold higher. *Lane 3* is the same as *lane 1* only 1 mM BS^3 was added for only 2 min instead of 30 min. *Lanes 4* and *5* are identical to *lanes 1* and *2*, respectively, except the VWF concentration was five times greater during the cross-linking step. *Lane 6* is identical to *lane 1* only DTT was added prior to BS^3 and Tris. Identical concentrations of VWF were loaded in each lane. *B*, experiments were performed identically to *A*, only the starting VWF consisted of higher molecular mass VWF multimers only (*lane 3*). 9.4 μg/ml VWF cross-linked with 1 mM BS^3 prior to reduction is shown in *lane 1*, whereas reduced VWF in the absence of cross-linker is present in *lane 2*. Data support the concept that binding interactions between different domains of VWF located on different monomer units may regulate protein solution conformation. Data are representative of >8 independent experiments with different donor pools.

Gd·HCl alters domain level features, and this is sufficient for VWF proteolysis. These observations were also validated using dynamic light scattering where neither addition of 1.25 M Gd·HCl nor Gd·DCl altered protein R_g (data not shown). In a control experiment (supplemental Fig. S3), we verified that 1.25 M Gd·DCl was as effective as 1.25 M Gd·HCl in increasing VWF susceptibility to proteolysis by ADAMTS-13. These experiments confirm that deuterated and hydrogenated forms of Gd·HCl are functionally similar.

Non-covalent Interactions between Different Monomers of VWF Stabilize Protein Quaternary Structure—The inability of Gd·HCl to alter R_g and previous reports of VWF self-association (14, 32) suggest that there may be molecular interactions between various domains within a single VWF multimer. To assess this, VWF was randomly cross-linked with homobifunctional cross-linker BS^3, which links proximal amine residues within the protein, prior to cleavage of intermonomer disulfide bonds using DTT and Western blot analysis (Fig. 6). As seen in *A*, cross-linking prior to reduction and blotting results in fragments with masses of 250, 500, and 750 kDa. In these studies, increasing the amount of cross-linker from 1 to 5 mM (*lane 1 versus 2* and *lane 4 versus 5*) did not markedly affect the pattern of multimers formed. Similarly increasing the ratio of VWF to BS^3 by altering VWF quantity (*lane 1 versus 4*, and *2 versus 5*) did not significantly affect the blot results. Even treatment with cross-linker for a brief 2 min (*lane 3*) instead of 30 min (*lane 1*) resulted in similar results, and these data together suggest that BS^3 cross-linking is a rapid process, and it likely stabilizes existing intramolecular binding interactions, rather than initiating new intermolecular interactions following Brownian collisions. In support of this, the negative control run, where VWF was treated with DTT prior to BS^3 addition, only resulted in a single 250-kDa band.

Whereas the maximum size of cross-linked VWF was 750 kDa when a pooled sample of VWF consisting of both low and high molecular mass protein fractions was used (Fig. 6*A*), larger units were observed in similar studies performed with only the higher molecular mass fraction (Fig. 6*B*). In the later studies, cross-linked units consisting of at least six monomer units were observed. Thus, the extent of cross-linking depends on the protein multimer distribution. The above cross-linking studies were also performed in the presence of 0.1% SDS, which disrupts most self-associated VWF (16). In these runs also, we observed the ladder pattern of cross-linked VWF shown in Fig. 6. Finally BS^3 treatment of dimeric ΔPro-VWF prior to blotting did not result in protein cross-linking as determined by Western blot analysis (data not shown). Because the intensity of cross-linked VWF (≥500 kDa) is typically greater than that of the monomer (250 kDa) in Fig. 6, the experiments suggest that interactions between the VWF domains located on different monomer units may be a "frequent" occurrence. Further, while the exact domains involved in the above interactions remains to be established, the occurrence of cross-linked units with >500 kDa (dimers) and the absence of cross-linking in runs with ΔPro-VWF is consistent with the notion that simple cross-linking of N terminus residues of VWF by BS^3 alone does not account for the observations. Overall, the intraprotein interactions revealed by studies with BS^3 may play a role in stabilizing VWF solution structure.

DISCUSSION

Small angle scattering experiments were performed to study the solution structure of VWF in the length scale from 2–250 nm. The results of this work complement previous crystallography studies of VWF, which have examined individual protein

TABLE 3
Protein dimensions obtained from ellipsoid fit of SANS data

	BSA	Fibrinogen	ΔPro-VWF	Multimer VWF
r_a (*nm*)	4.4	26	70	175
r_b (*nm*)	2.3	2.7	9.1	28
Aspect ratio ($=r_a/r_b$)	1.9	9.63	7.7	6.2
R_g (*nm*)	2.5	16.9	31.8	80.2
Mass (kDa)	137.1	387.4	429.6	– [a]
Ellipsoid volume occupied by protein (% v/v)	97.6	34.7	2.0	1.6

[a] Reliable mass values for multimeric VWF could not be obtained from SANS data because of its large size.

domains at smaller length scales (16, 29). Some of the gross structural features of VWF are presented in Table 3, where they are compared with our unpublished SANS results from two other proteins, BSA and human fibrinogen. Here, it is seen that all proteins can be modeled as prolate ellipsoids. This is in general agreement with the prediction of Kuhn (33) who suggested that the overall shape of a polymeric macromolecule undergoing random walk is aspherical. In the case of proteins, secondary and tertiary interactions between amino acid side chains likely cause the formation of ellipsoids with distinct aspect ratios. Thus protomer and multimer VWF have an aspect ratio of ~6–7. Fibrinogen is more elongated, and this is consistent with its crystal and electron microscopy structure (34, 35). BSA used in this study appears to be predominantly in the form of a dimer and appears more compact to the neutron beam compared with other proteins (36). The I_0 values from neutron scattering studies were used to estimate protein mass as discussed under supplemental materials, and these are in agreement with published data. The volume fraction of the ellipsoid occupied by both the protomer and multimeric forms of VWF was low (~1.6–2%) compared with the other proteins.

With regard to the substructural levels within VWF, three levels were consistently observed in the multimeric protein. Whereas VWF polydispersity affected the G_1 or I_0 values in the first structural level, the smaller substructures were similar and did not display any obvious differences among donors with different blood groups. These include the entire multimeric protein with R_g of ~75 nm, the globular domain with R_g of ~16 nm and mass fractal-like domain level structures with R_g of 4.5 nm. Similar to this, two structural levels were observed in the protomeric VWF including the overall dimeric protein with R_g of 30 nm and domains of 4.5 nm. The smaller domains noted above may correspond to individual functional units that have been previously crystallized (16). They may also contain information on the arrangement of individual domains in clusters. SANS data of comparable concentrations of multimeric and protomeric VWF are overlaid in supplemental Fig. S4, and these data match at $q > 0.3$/nm. Because lower mass (~40 kDa, Fig. 2*B*) contaminating proteins seen in SDS-PAGE runs are expected to affect scattering data at $q > 1.5$ nm (size range of 4 nm) and because the scattering of multimeric and protomer VWF is similar in this q range, the results in supplemental Fig. S4 confirm that low mass molecules have only minor contribution to SANS experiments.

The structural features reported in this article likely represent those of native human VWF in blood plasma, because our macromolecules are functional. In this regard, both the recombinant and purified multimeric forms of VWF had the ability to bind platelet GpIb under fluid shear, and recombinant factor VIII in cytometry/clotting assays. Mulitimeric protein was also not denatured upon isolation, because the protease ADAMTS-13 did not cleave this protein unless denaturant Gd·HCl was added to alter protein conformation and expose sites of proteolysis.

This study presents evidence that individual domains on distinct VWF monomer units may interact in a non-covalent manner. In support of this, we observed that cross-linking VWF with BS^3 results in the formation of stable amide bonds linking proximal amino acid residues on different monomer units. Previous studies also provide evidence of interactions between VWF units under static (15, 32) and fluid flow conditions (14, 37). In a study performed with 2-mercaptoethanol-reduced VWF (15), the authors report that protomer VWF may spontaneously self-associate in solution when they are at concentrations of >100 μg/ml, and that such binding is dissociated upon addition of 0.1% SDS. Based on our observation that ΔPro-VWF exhibits a sharp peak in dynamic light scattering studies over a range of solution concentrations, we suggest that the dimeric protein may not spontaneously aggregate. Thus, independent mechanisms may regulate the association of 2-mercaptoethanol-treated and non-denatured proteins. In other studies, non-denatured recombinant and plasma VWF in solution have been shown to bind surface immobilized VWF under fluid shear (37) and under static conditions (32). Further, VWF self-associates in suspension upon application of fluid shear (14). Although the detailed mechanisms of these interactions are not yet established, it is suggested that VWF self-association is specific in nature (32), and that it involves at least two different epitopes located on distinct portions of VWF. Further, these interactions do not involve the homotypic interaction between the A1 and A3 domains (37). Finally, VWF self-association can be partially dissociated by 0.1% SDS (14). In the current study, while addition of 0.1% SDS during the VWF cross-linking step did not prevent the action of the BS^3 linker, it is noted that the conformation of VWF in these studies is also constrained by disulfide linkages between monomer units. Overall, more detailed investigations in the future may reveal whether similar or distinct mechanisms contribute to the different observations of VWF-VWF interaction described above. Further, it remains to be established to what degree the interactions between the domains contribute to protein ellipsoidal shape and function.

The exact protein interactions stabilized by BS^3 in the cross-linking studies remains to be established, though our experiments suggest that these do not simply involve the linkage of proximal primary amines located near the N terminus of VWF. Further, since protein crosslinking was observed to occur frequently and yet amino acids only occupied ~2% of the VWF volume, it may be possible that these interactions stabilized by BS^3 are specific in nature. This hypothesis is the subject of current investigations in our laboratory.

In our studies using light and neutron scattering, we did not observe changes in the R_g of VWF upon addition of 1.25 M Gd·HCl or deuterated Gd·DCl. In contrast it has been noted that several smaller and more compact proteins including

α-tryptophan synthase (38), cytochrome *c* (39), decorin (40), creatine kinase (41), RNaseA (42), and lysozyme (43) to name a few, change their R_g upon addition of 0.3–8 M Gd·HCl. It is perhaps not surprising that addition of Gd·HCl did not change VWF radius, because this protein is loosely packed (Table 3). A recent study suggests that denatured proteins behave as a random coil and that there exists a power law relationship between the number of amino acid residues and R_g (44). Upon extrapolating the findings of this article to the 4100 amino acid ΔPro-VWF, it can be predicted that even complete denaturation of this protein is not likely to yield a greater R_g value. Structural changes at length scales <10 nm were however apparent in our study. These changes at small length scales appear to increase the susceptibility of VWF to proteolytic cleavage in the presence of ADAMTS-13 similar to a previous report (8).

Previous studies have shown that fluid shear enhances the binding of VWF to platelets (45), and that it facilitates VWF proteolysis by ADAMTS-13 (9). The force applied to the protein even at the highest shear rates in these experiments is small, ~0.1 pN (46). In support of the proposition that shear causes large scale changes in protein conformation, surface-immobilized VWF has been shown to extend from a globular to an unfolded state upon application of fluid shear (47). Others suggest, however, that this observation may be substrate specific because VWF immobilized on collagen does not undergo similar changes in response to fluid flow (48). In support of the proposition that subtle changes are sufficient for functional alterations, x-ray studies show how point mutations in the A1-domain and GpIb receptor enhance VWF-GpIb binding affinity, without dramatically altering protein structure (19). We have also observed in studies that measure VWF solution structure changes in real time using SANS that the protein undergoes conformation changes at small length scales upon application of hydrodynamic stress.[3] Besides, large scale conformation changes and subtle changes to individual domains, it has recently been shown that ADAMTS-13 proteolysis of VWF is enhanced following the binding of platelet GpIbα to VWF A1 domain (49). These authors suggest that the A1 domain of VWF inhibits cleavage of the A2 domain, and that this inhibition is relieved by binding with platelet GPIb. Thus, interactions between the domains of VWF may be important functional regulators of protein function. The role of Gd·HCl in our studies may thus be to relieve these interactions between the A2 and other domains, thereby facilitating the action of ADAMTS-13.

Whereas the exact nature of the arrangement of domains and their response to biochemical/physical stimulus is under investigation, the present data are consistent with a model where VWF multimers are formed by strong hydrophobic interactions between different domains of the protomers, which can keep this protein in a passive form. Fluid shear and surface immobilization may cause subtle changes in the protein structure that expose hitherto masked domains. Finally, the current article establishes small angle scattering tools for the study of blood proteins, which may be valuable in future studies of protein domain-domain interactions.

[3] I. Singh, L. Porcar, and S. Neelamegham, manuscript in preparation.

Acknowledgments—We thank Dr. Gian P. Visentin for reviewing and providing critical comments on this manuscript. We also thank Lionel Porcar for discussions about SANS experiments. The NIST neutron research facility used in this work is supported in part by the NSF under agreement DMR-0454672. We acknowledge support of the NIST, US Department of Commerce, in providing the neutron facilities used in this work.

REFERENCES

1. Sadler, J. E. (1998) *Annu. Rev. Biochem.* **67,** 395–424
2. Kroll, M. H., Hellums, J. D., McIntire, L. V., Schafer, A. L., and Moake, J. L. (1996) *Blood* **88,** 1525–1541
3. Wagner, D. D., Olmsted, J. B., and Marder, V. J. (1982) *J. Cell Biol.* **95,** 355–360
4. Savage, B., Saldivar, E., and Ruggeri, Z. M. (1996) *Cell* **84,** 289–297
5. Doggett, T. A., Girdhar, G., Lawshe, A., Schmidtke, D. W., Laurenzi, I. J., Diamond, S. L., and Diacovo, T. G. (2002) *Biophys. J.* **83,** 194–205
6. Kasirer-Friede, A., Cozzi, M. R., Mazzucato, M., De Marco, L., Ruggeri, Z. M., and Shattil, S. J. (2004) *Blood* **103,** 3403–3411
7. Levy, G. G., Nichols, W. C., Lian, E. C., Foroud, T., McClintick, J. N., McGee, B. M., Yang, A. Y., Siemieniak, D. R., Stark, K. R., Gruppo, R., Sarode, R., Shurin, S. B., Chandrasekaran, V., Stabler, S. P., Sabio, H., Bouhassira, E. E., Upshaw, J. D., Jr., Ginsburg, D., and Tsai, H. M. (2001) *Nature* **413,** 488–494
8. Tsai, H. M. (1996) *Blood* **87,** 4235–4244
9. Tsai, H. M., Sussman, II, and Nagel, R. L. (1994) *Blood* **83,** 2171–2179
10. Slayter, H., Loscalzo, J., Bockenstedt, P., and Handin, R. I. (1985) *J. Biol. Chem.* **260,** 8559–8563
11. Ohmori, K., Fretto, L. J., Harrison, R. L., Switzer, M. E., Erickson, H. P., and McKee, P. A. (1982) *J. Cell Biol.* **95,** 632–640
12. Fowler, W. E., Fretto, L. J., Hamilton, K. K., Erickson, H. P., and McKee, P. A. (1986) *J. Clin. Investig.* **76,** 1491–1500
13. Raghavachari, M., Tsai, H., Kottke-Marchant, K., and Marchant, R. E. (2000) *Colloids Surf. B Biointerfaces* **19,** 315–324
14. Shankaran, H., Alexandridis, P., and Neelamegham, S. (2003) *Blood* **101,** 2637–2645
15. Loscalzo, J., Fisch, M., and Handin, R. I. (1985) *Biochemistry* **24,** 4468–4475
16. Emsley, J., Cruz, M., Handin, R., and Liddington, R. (1998) *J. Biol. Chem.* **273,** 10396–10401
17. Celikel, R., Ruggeri, Z. M., and Varughese, K. I. (2000) *Nat. Struct. Biol.* **7,** 881–884
18. Fukuda, K., Doggett, T. A., Bankston, L. A., Cruz, M. A., Diacovo, T. G., and Liddington, R. C. (2002) *Structure* (*Camb.*) **10,** 943–950
19. Huizinga, E. G., Tsuji, S., Romijn, R. A., Schiphorst, M. E., de Groot, P. G., Sixma, J. J., and Gros, P. (2002) *Science* **297,** 1176–1179
20. Calmettes, P., Roux, B., Durand, D., Desmadril, M., and Smith, J. C. (1993) *J. Mol. Biol.* **231,** 840–848
21. Wise, R. J., Pittman, D. D., Handin, R. I., Kaufman, R. J., and Orkin, S. H. (1988) *Cell* **52,** 229–236
22. Fischer, B. E., Schlokat, U., Reiter, M., Mundt, W., and Dorner, F. (1997) *Cell Mol. Life Sci.* **53,** 943–950
23. Xiao, Z., Goldsmith, H. L., McIntosh, F. A., Shankaran, H., and Neelamegham, S. (2006) *Biophys. J.* **90,** 2221–2234
24. Glinka, C. J., Barker, J. G., Hammouda, B., Krueger, S., Moyer, J. J., and Orts, W. J. (1998) *J. Apply Crystallogr.* **31,** 430–445
25. Spalla, O. (2002) *Neutrons, X-Rays and Light Scattering Methods Applied to Soft Matter*, 1st Ed., pp. 23–50, Elsevier, New York
26. Calmettes, P., Durand, D., Desmadril, M., Minard, P., Receveur, V., and Smith, J. C. (1994) *Biophys. Chem.* **53,** 105–113
27. Beaucage, G. (1996) *J. Appl. Crystallogr.* **29,** 134–146
28. Saenko, E., Sarafanov, A., Greco, N., Shima, M., Loster, K., Schwinn, H., and Josic, D. (1999) *J. Chromatogr. A.* **852,** 59–71
29. Bienkowska, J., Cruz, M., Atiemo, A., Handin, R., and Liddington, R. (1997) *J. Biol. Chem.* **272,** 25162–25167

30. Jacrot, B. (1976) *Rep. Progr. Phys.* **39,** 911–953
31. Bendetowicz, A. V., Wise, R. J., and Gilbert, G. E. (1999) *J. Biol. Chem.* **274,** 12300–12307
32. Ulrichts, H., Vanhoorelbeke, K., Girma, J. P., Lenting, P. J., Vauterin, S., and Deckmyn, H. (2005) *J. Thromb. Haemost.* **3,** 552–561
33. Kuhn, W. (1934) *Kolloid-Z* **68,** 2–11
34. Yang, Z., Kollman, J. M., Pandi, L., and Doolittle, R. F. (2001) *Biochemistry* **40,** 12515–12523
35. Hall, C. E., and Slayter, H. S. (1959) *J. Biophys. Biochem. Cytol.* **5,** 11–16
36. Wen, J., Arakawa, T., and Philo, J. S. (1996) *Anal. Biochem.* **240,** 155–166
37. Savage, B., Sixma, J. J., and Ruggeri, Z. M. (2002) *Proc. Natl. Acad. Sci. U. S. A.* **99,** 425–430
38. Gualfetti, P. J., Iwakura, M., Lee, J. C., Kihara, H., Bilsel, O., Zitzewitz, J. A., and Matthews, C. R. (1999) *Biochemistry* **38,** 13367–13378
39. Segel, D. J., Fink, A. L., Hodgson, K. O., and Doniach, S. (1998) *Biochemistry* **37,** 12443–12451
40. Scott, P. G., Grossmann, J. G., Dodd, C. M., Sheehan, J. K., and Bishop, P. N. (2003) *J. Biol. Chem.* **278,** 18353–18359
41. Zhou, J. M., Fan, Y. X., Kihara, H., Kimura, K., and Amemiya, Y. (1997) *FEBS Lett.* **415,** 183–185
42. Sosnick, T. R., and Trewhella, J. (1992) *Biochemistry* **31,** 8329–8335
43. Hoshino, M., Hagihara, Y., Hamada, D., Kataoka, M., and Goto, Y. (1997) *FEBS Lett.* **416,** 72–76
44. Kohn, J. E., Millett, I. S., Jacob, J., Zagrovic, B., Dillon, T. M., Cingel, N., Dothager, R. S., Seifert, S., Thiyagarajan, P., Sosnick, T. R., Hasan, M. Z., Pande, V. S., Ruczinski, I., Doniach, S., and Plaxco, K. W. (2004) *Proc. Natl. Acad. Sci. U. S. A.* **101,** 12491–12496
45. Goto, S., Salomon, D. R., Ikeda, Y., and Ruggeri, Z. M. (1995) *J. Biol. Chem.* **270,** 23352–23361
46. Shankaran, H., and Neelamegham, S. (2004) *Biophys. J.* **86,** 576–588
47. Siedlecki, C. A., Lestini, B. J., Kottke-Marchant, K. K., Eppell, S. J., Wilson, D. L., and Marchant, R. E. (1996) *Blood* **88,** 2939–2950
48. Novak, L., Deckmyn, H., Damjanovich, S., and Harsfalvi, J. (2002) *Blood* **99,** 2070–2076
49. Nishio, K., Anderson, P. J., Zheng, X. L., and Sadler, J. E. (2004) *Proc. Natl. Acad. Sci. U. S. A.* **101,** 10578–10583